Project	AtlantOS – 633211
Deliverable number	D7.14
DOI	10.13155/55475
Deliverable title	Current EOV Report
Description	Merged satellite/in-situ surface current products and impact of AtlantOS observations
Work Package number	WP7
Work Package title	Data flow and data integration: product development (EOV based assessment)
Lead beneficiary	CLS
Lead authors	H. Etienne, M.-H. Rio (CLS)
Contributors	L. Petit de la Villeon (Ifremer), F. Gourtay-Le Hingrat (Ifremer)
Submission data	08/06/2018
Due date	31/03/2018
Comments	We faced minor technical problems and needed more time to investigate further some data processing

Stakeholder engagement <u>relating to this task</u>

WHO are your most important stakeholders?	X Private company (SME) X National governmental body
WHERE is/are the company(ies) or organization(s) from?	X Your own country (France)
Is this deliverable a success story? If yes, why? **If not, why?**	Yes, because we show the feasibility of the satellite/in-situ merging and the ability of the ATLANTOS SADCP data to be used in model validation process
Will this deliverable be used? **If yes, who will use it?** **If not, why will it not be used?**	Yes, because this is a starting point to what can be done with the ATLANTOS in-situ observations of the ocean velocity.

List of contents

List of figures

1. Introduction

As written in the description of work, the objective of this subtask is to demonstrate the value of the in-situ surface currents observing system by ensuring the link with the ESA GlobCurrent project. GlobCurrent is an ESA Data User Element started in October 2013 (running until June 2017) whose objective is "to advance the quantitative estimation of ocean surface currents from satellite sensor synergy and demonstrate impact in user-led scientific, operational and commercial applications that, in turn, will increase the uptake of satellite measurements".

In the framework of Globcurrent, several surface and near-surface current products have been calculated. First, global, ¼ maps of ocean surface geostrophic currents (from altimetry), Ekman currents at two distinct depths (surface and 15m) and combined Geostrophic+Ekman currents at 0 and 15m depth have been calculated for the period January 1993 - May 2016. Temporal resolution of the products is daily for the geostrophic component and 3-hourly for the Ekman and combined geostrophic+Ekman component (Rio et al, 2014). The Ekman currents have been calculated at two levels (surface and 15m) using an empirical approach. In addition, a study has been carried out to reconstruct the 3D profile of the Ekman current in the Ekman layer, either based on the empirical approach, or by developing an analytical model of the Ekman response to wind speed (Tanne, 2016). This former approach is adapted from the calculation of the Ekman currents in the OSCAR products (Bonjean et al, 2002).

In a first chapter, we will calculate merged SSH/SST velocity maps over the AtlantOS region for a period with a satisfying drifting buoy coverage and compare them to the AtlantOS drifting buoy velocities.

The merged SSH/SST currents could finally be combined to the AtlantOS drifter velocities through a multivariate analysis approach to further improve the ocean surface current retrieval. This method is currently developed in the framework of the CNES DUACS-MR project.

In a second chapter, we explore the SISMER SADCP (Shipboard Acoustic Doppler Current Profiler, IFREMER /IDM/SISMER) database to assess the possibility to extract a wind driven component from the measured velocity to compare with an Ekman model and the use of these in-situ data for model validation.

2. Synergy Globcurrent/Drifting buoys

Three years (2014-2016) of merged SSH/SST surface currents have been calculated in the frame of the Globcurrent project. In this task we have validated these currents for the Atlantic Ocean through comparison to drifting buoy velocities. We have used in-situ velocities deduced from the trajectories of all the 15m drogued SVP (Surface Velocity Program) drifters available in the Atlantic Ocean over that period. Figure 1 shows the trajectories of available drifters.

2.1. Method

The method used to calculate the optimally merged SSH/SST velocities (uopt, vopt) consists in inverting the heat conservation equation for the velocity (u,v) by using the altimeter derived geostrophic velocities as background information (ubck, vbck). The method is fully described in Rio et al (2016) and Rio and Santoleri (submitted to RSE).

Altimeter data used are the daily, ¼ gridded maps of geostrophic currents calculated at CLS in the framework of the Ssalto-Duacs project and distributed by the Copernicus Marine Environment Monitoring Service (CMEMS) Sea Level Thematic Assembly Center (TAC). Two different products were used, the "twosat" product calculated using information from only two altimeter satellites, and the "allsat" product obtained using all altimeter data available at a given time.

Sea Surface Temperature maps were downloaded from the Remote Sensing System (REMSS) website. Two products are available, at a daily temporal resolution: a low-resolution product (25 km) based on microwave SST observations (TMI, AMSR-E, AMSR2 and WindSat and GMI after 2014), hereafter the MW SST product, and a higher resolution product (9 km) based on the combination of microwave and infrared (Terra MODIS, Aqua MODIS) data, hereafter the MWIR SST product.
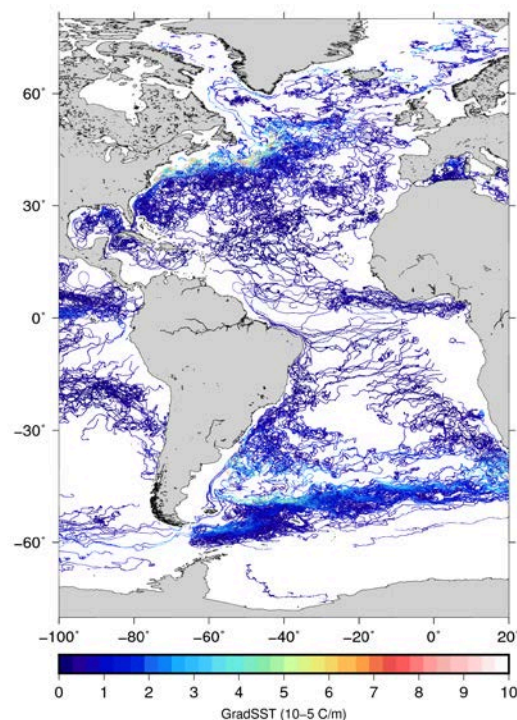
Figure 1: Trajectories of SVP drogued drifters in the Atlantic Ocean for the period 2014-2016. Colors are for the amplitude of the spatial SST gradient (REMSS products) interpolated at the buoy times and positions.

6

2.2. Results

An example of the merging capability of the method is shown on Figure 2. The plots show a cyclonic eddy in the Gulfstream area on March 24th, 2015 as resolved by the different surface current products (black arrows).

Underlying colors correspond to the REMSS MW SST product. In the "twosat" altimeter velocities field (Figure 2a) the eddy features an elongated structure on its southern east side which is not consistent with the underlying SST field. The "allsat" altimeter velocity field (Figure 2c) benefits from observations from additional altimeter tracks and successfully manages to resolve this structure. By combining the "twosat" altimeter velocities and the MW SST data, the shape of the eddy is modified, and the optimal velocities are in very good agreement with both the "allsat" velocities and the SST image (Figure 2b). Further improvement is obtained by combining the "allsat" altimeter velocities and the MWIR SST data (Figure 2e).

This example highlights the efficiency of the method to add significant short scale information where altimeter tracks are insufficient to allow for the correct restitution of mesoscale eddies in altimeter maps.
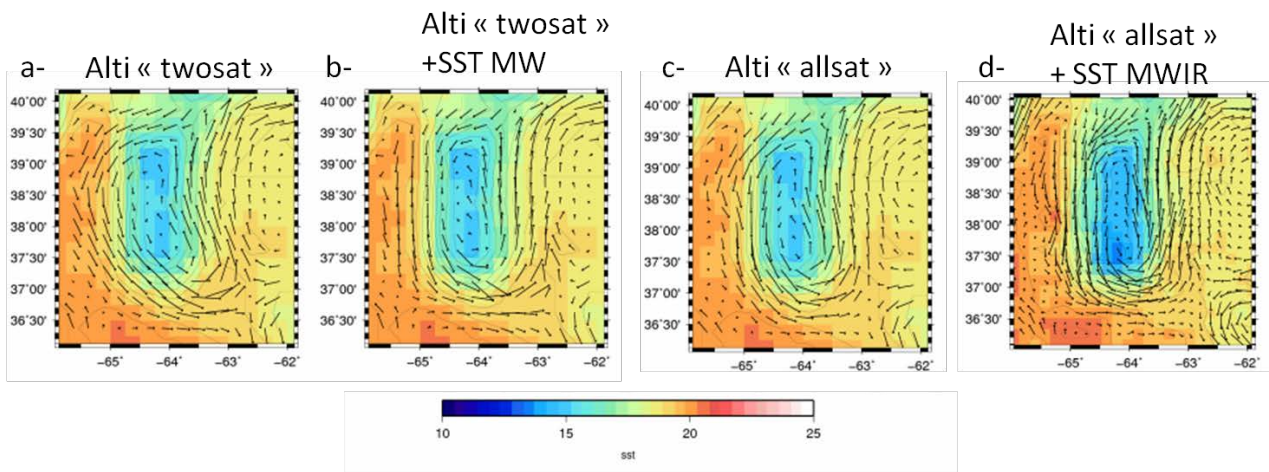
Figure 2: Example on March 24th, 2015 in the Gulfstream area: a- "twosat" background velocities, b- optimal velocities using the "twosat" altimeter velocities as background, c- "allsat" velocities and d- optimal velocities using the "twosat" altimeter velocities as background. Colors in a-, b- and c- correspond to the MW SST product (25 km resolution), and colors in d- are from the MWIR SST product (9 km resolution).

Both the altimeter derived geostrophic velocities and the optimally combined SSH+SST velocities were then interpolated along the trajectory of the 15m drogued drifters and Root Mean Square (RMS) differences and correlation coefficients were calculated between both components of the in-situ drifter velocities and the corresponding altimeter and optimal velocities. We then further quantify the method efficiency by calculating a percent of improvement (U_{impr} and V_{impr}) for both components of the velocity as follows:

$$U_{impr} = 100 * (1 - (RMSU_{opt} / RMSU_{bck})^2)$$

$$V_{impr} = 100 * (1 - (RMSV_{opt} / RMSV_{bck})^2)$$

First, RMS differences and correlation coefficients were calculated in 1°C/m bins of SST spatial gradient amplitude. The value of this amplitude interpolated along the buoy trajectories is given on Figure 1. SST

gradients range from 0 in low variability areas to $7\text{-}8.10^{-5}$ °C/m in western boundary currents (Gulfstream, Falkland current, ACC). Figure 3 shows the results over the global Atlantic Ocean.

The first expected result is that the "allsat" altimeter geostrophic velocities (blue line) compare better to the drifter velocities than the "twosat" altimeter velocities (black line) in all SST gradients bins: RMS differences to drifting buoy velocities are systematically reduced. In 2014-2016, the "allsat" altimeter products are based on data from 5 satellites compared to only 2 for the "twosat" products, so that we expect higher spatial resolution to be achieved in this product, and hence better agreement with in-situ drifting buoy velocities.
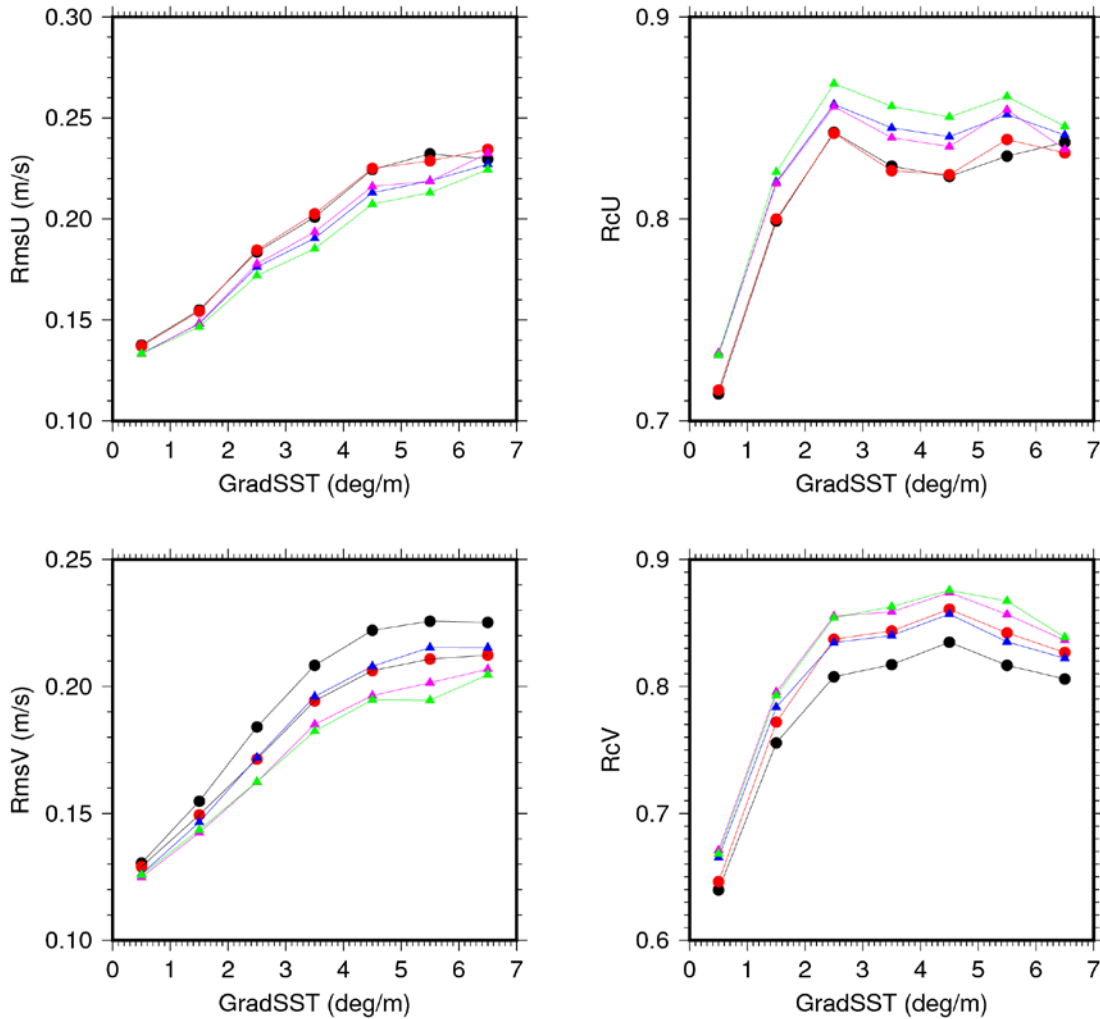
Figure 3: zonal (top) and meridional (bottom) Root Mean Square differences in m/s (left) and correlation coefficient (right) between the drifter velocities and (black) the "twosat" altimeter velocities, (blue) the "allsat" altimeter velocities, (red) the optimal "twosat"+MW SST velocities, (pink) the optimal "allsat"+MW SST velocities and (green)) the optimal "allsat"+MWIR SST velocities . The RMS values are obtained for SST spatial gradients (GradSST) ranging from 0 to 7.10^{-5} °C/m.

Significant improvement is obtained for the meridional component of the velocity by merging the altimeter velocities and the MW SST product for SST gradients greater than 2.10-5°C/m. The comparison to drifting buoy velocities is equivalent to the result obtained using the "allsat" altimeter velocities (red and blue lines are superimposed both for the RMS and for the correlation coefficient). On the contrary, no significant difference is observed for the zonal component between the "twosat" altimeter velocities and the optimally merged "twosat"+MWSST velocities. RMS differences and linear correlation coefficients to the drifter velocities are unchanged (the black and red curves are superimposed).

As discussed in Rio et al., 2016, the reduced ability of the method to correct the zonal altimeter velocity component compared to the meridional component is expected. It is due to two main factors:

- First, altimeter tracks are oriented North-South. Consequently, the meridional (i.e. close to along-track) component of the background velocities is less accurate than the zonal (i.e close to across-track) component and the corrective term from SST is consequently potentially stronger.
- Second, SST gradients in the ocean are predominantly zonal, and our approach provides by construction a correction term in the across SST front direction (=meridional component of the currents).

For these two reasons we expect the correction term on the zonal velocities calculated by our approach to be small and therefore more sensitive to the accuracy of the SST product and the forcing term estimate.

We now focus on the efficiency of our method to improve the "allsat" altimeter geostrophic velocities. The "allsat" velocities are based on all altimeter data available at a given time. They are therefore the best global ocean geostrophic current product presently available.

Further significant improvement is obtained on the meridional component by merging the "allsat" altimeter velocities and the MW SST information (pink line is below the blue line for the RMS and above the blue line for the correlation), meaning that merging SST and altimeter measurements allows to improve our knowledge of the ocean currents at 15m depth compared to the use of the state-of-the-art "allsat" altimeter product.

As for the "twosat" case, no significant difference is obtained on the zonal component between the "allsat" and the optimally merged "allsat"+MWSST velocities (the blue and pink curves are superimposed).

However, the higher resolution MWIR SST product provides significant information to correct also the zonal altimeter velocity component. The green line is below the blue line on the RMS plot for the zonal component and above the blue line for the correlation coefficient.

We now analyze the percent of improvement calculated in 20° by 20° boxes. Results are shown on Figure 4. Circles correspond to boxes where the RMS differences to buoy velocities obtained with one product or the other are not significantly different at the 90% level. Result analysis is based on the fully coloured boxes, where we consider the calculated RMS differences obtained using one velocity or the other to be significantly different.

These plots allow refining the general performance analysis given before. We see that the performance is not homogeneous for the zonal component (top left plot). While improvement is negative (degradation) at high latitudes, we obtain a few percent of improvement in the other boxes.

When focussing on SST gradients greater than 1.10^{-5}°C/m (middle left plot), results obtained for the zonal component using the MW SST product are not very good (not significantly different or a slight degradation is obtained). This is much improved when using the higher resolution MW+IR SST product (bottom left plot). Around 5% of improvement is obtained in many boxes, also at high latitudes.

It is interesting to see a positive improvement value in the Benguela upwelling system area (West of the South-western African coast). In this area, northward winds along the South-western African coast result in Ekman transport offshore and consequent upwelling of cold and nutrient-rich waters that sustain the very active Benguela ecosystem. Being ageostrophic, Ekman currents are not resolved by altimeter derived surface currents. On the other hand, such upwelling systems are clearly visible on SST images which might consequently bring significant additional information to altimetry (see the example based on model outputs in Rio et al, 2016).

Positive, significant improvements are obtained everywhere for the meridional component of the velocity (right plots on Figure 4). Maximum improvement is obtained when SST spatial gradient amplitude is greater than 1.10-5 °C/m (middle and low plots) in the equatorial band (up to 30-40%) and in western boundary currents (10-20%).
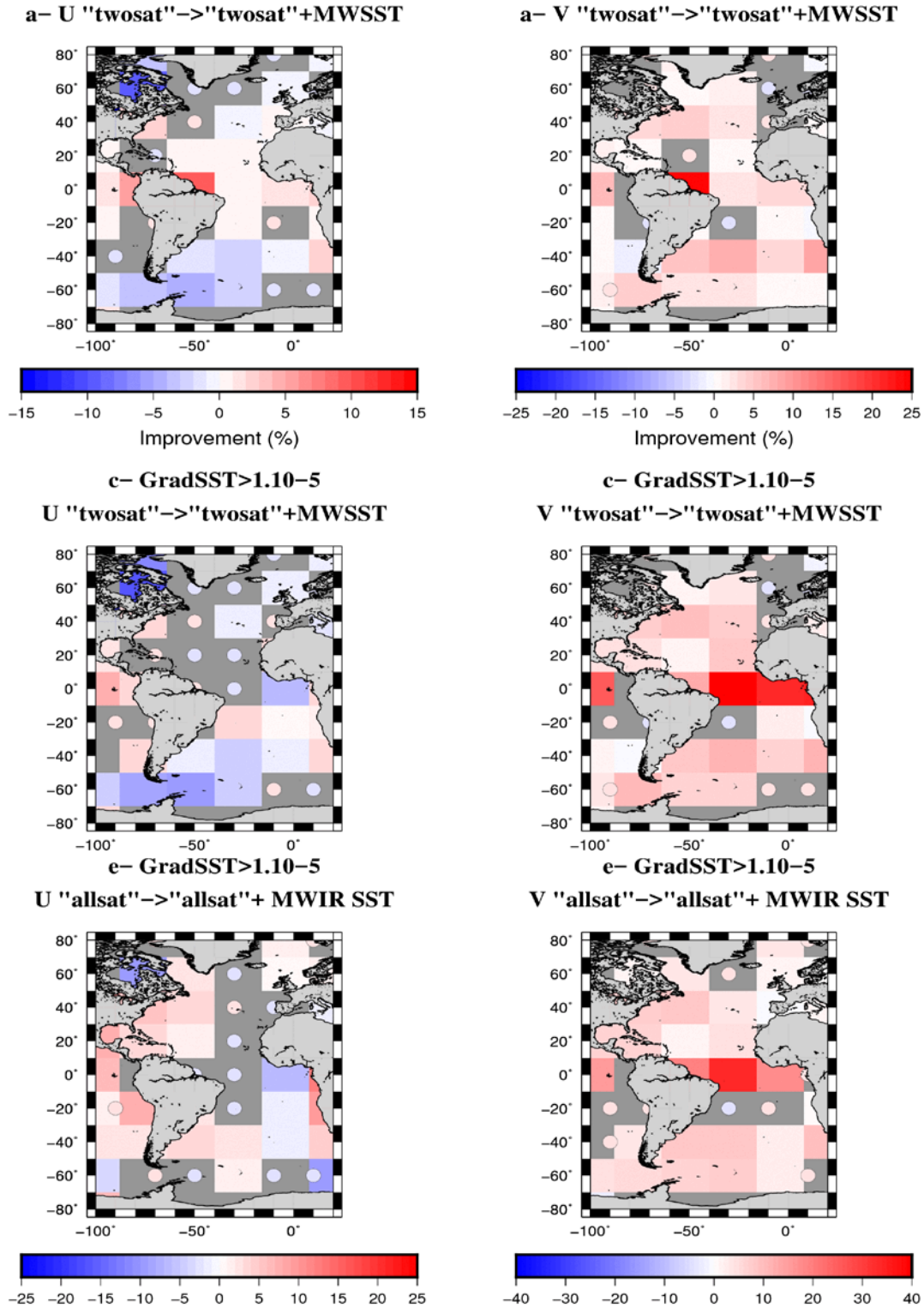
Figure 4: % of improvement obtained for the zonal (left) and meridional (right) component of the velocity using (top) the "twosat" + MW SST velocities compared to the "twosat" velocities, (middle)- same but for SST gradients greater than 10^{-5}°C/m, (bottom) the "allsat"+MWIR SST velocities compared to the "allsat" velocities. Circles correspond to boxes where the RMS differences to buoy velocities obtained with one product or the other are not significantly different at the 90% level.

10

3. ATLANTOS SADCP

3.1. Data inventory

An inventory of the available SADCP and moored ADCP has been made from the SISMER database. Duration of the time series, upper most depth, vertical resolution and frequency of the data has been checked to evaluate the consistency of these observations with the observation of an Ekman spiral. Hence, ocean current in the first 100m are ideally required, with upper level in the first 20 meters. Moreover, extratropical data are suitable. Most of the data selected comes from SADCP, while moored ADCP are meanly in tropical area or deep measurements.

Continuous processing of ADCP data collected on board French vessels are performed. The following map (Figure 5) represents the data available through the Ifremer / Sismer database (see also Appendix A -).

2001-2017

2012

Figure 5: top: ADCP data collected during the period 2001-2017 and further processed, bottom: ADCP data collected in 2012 (note data along the Pacific Ocean)

Note that the geographical coverage can vary from one year to another depending on the cruise plans. Most of the data have been collected in the Atlantic Ocean but long transects along the Pacific Ocean (Year 2012) also exist.

The ADCP data from 530 cruises are publicly available through the Ifremer / Sismer database.

The whole dataset is described on http://doi.org/10.12770/60ad1de2-c3e1-4d33-9468-c7f28d200305 and each year of data is described using a specific DOI (see related pages in the previous landing page). All the data (OceanSites format) are available on an ftp site:ftp://ftp.ifremer.fr/ifremer/coriolis/adcp/.

All the ADCP data have been loaded in the Coriolis database (ingestion) and there is an ongoing work on how to distribute the data and make them visible through the selection tool: http://www.coriolis.eu.org/Data-Products/Data-Delivery/Data-selection.

The objectives of the ongoing developments are to make data easily available, and to eventually propose collocated ADCP data with other data (altimetry).

In the next months we will explore the possibility to enlarge the ADCP dataset by adding the data available at the University of Hawai (GO-SHIP ADPC data).

For the specific AtlantOS study, the 2010 to 2015 period has been selected. 231 ADCP have been recovered from the SISMER database (Figure 6) between 2010 and 2015. These data are high frequency measurements (until 2 minutes frequency). Considering the vertical sampling, we have to check each SADCP to estimate if the Ekman component can be observed. Indeed, there is no so much measurements in the first 20m of the ocean (Figure 7), and the first depth sampled by many SADCP can be even deeper. 30 SADCP have the first measurement between 12 and 15m, 90 between 15 and 20m. This might be a limit for the analysis on Ekman current vertical structure.

Indeed, the Ekman depth depends on the latitude, the wind speed and the ocean stratification. In unstratified layers, typical value of the Ekman depth at 45°N and with a 10 m/s wind speed is 50m. This value further decreases with increasing stratification. Consequently, we are not expecting to observe the whole Ekman spiral from all the SADCP. Moreover, some SADCP won't be able to observe the Ekman spiral at all, depending on their trajectory and their vertical sampling.

A careful analysis of the expected Ekman depth values along each SADCP trajectory has been done to select the relevant data for this study. Hence, only **61 SADCP have been selected,** considering:

- First level of measurement in the upper 20m;
- At least 1 SADCP level in the Mixed Layer Depth (MLD) as computed by the Global ARMOR3D L4 products (CMEMS product)
- Nearly continue SADCP time series longer than 4 days.

These SADCP are listed in Appendix B -

Figure 6: Tracks of the 2010-2015 SADCP from SISMER

Figure 7: Depth sampled by the 2014-2015 SADCP (10m bins)
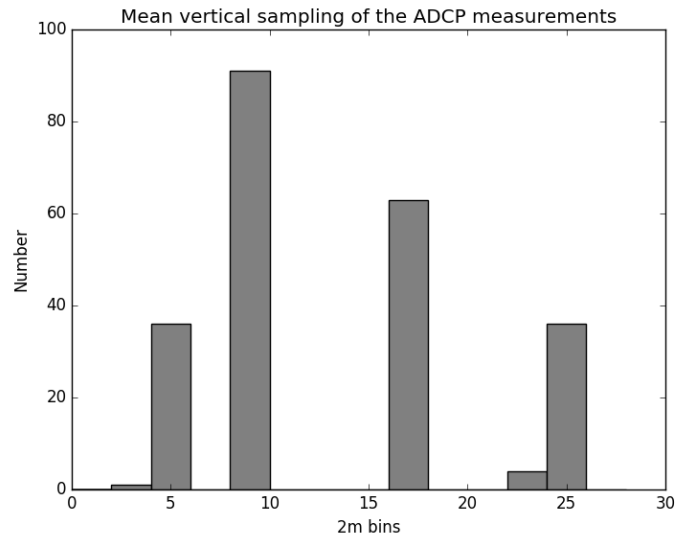
Figure 8: Vertical resolution of the 2014-2015 VM-ADCP (2m bins)

3.2. SADCP wind driven signal

Most of the time, the lack of datasets that sampled the upper ocean with vertical resolution sufficient to capture the vertical structure of the Ekman current avoids isolating the Ekman flow. Moreover, time series are generally not long enough to resolve wind-driven flow relative to much larger pressure-driven flows. The traditional approach in analyzing upper-ocean currents has been to subtract a deep ''reference'' velocity to isolate the local wind-driven flow (Davis et al. 1981; Price et al. 1987; Weller et al. 1991). This method assumes that the pressure-driven flows are vertically uniform above the reference depth. Price et al. (1987) introduced a wind-coherent ensemble average that greatly improved su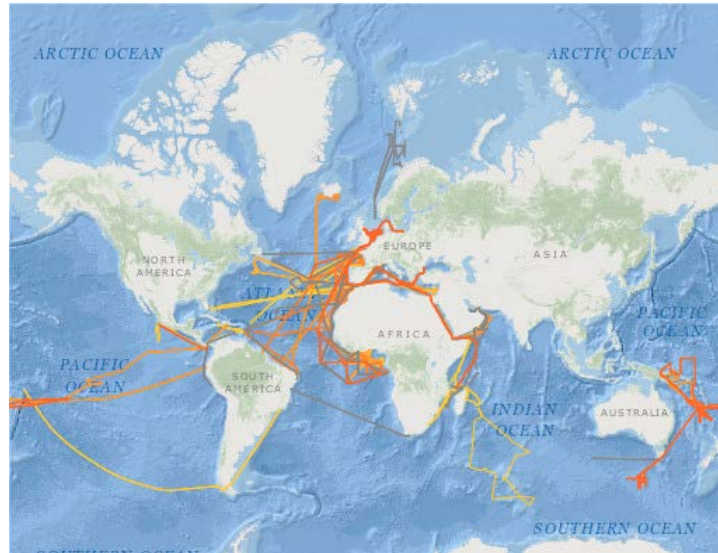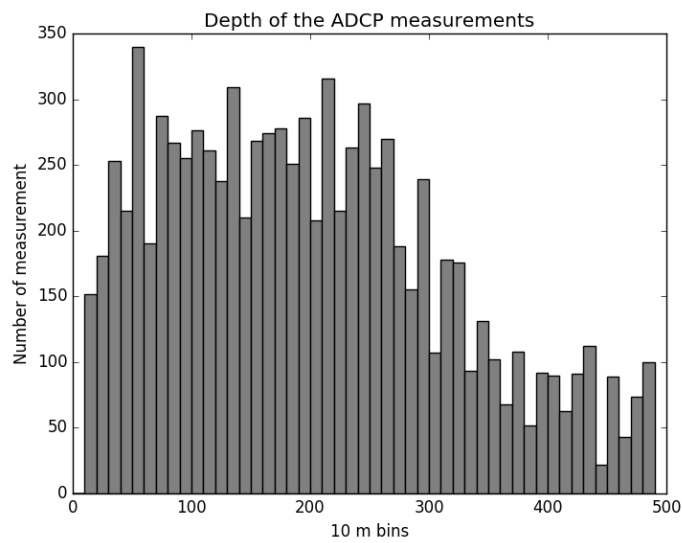ccess in isolating the Ekman signal. But, it is based on averaging over a long record (160 days) on moored Current Meters (Long Term Upper Ocean Study LOTUS 3). This approach has since been shown to enhance the Ekman signal in many datasets (Weller et al. 1991; Wijffels et al. 1994, Lee and Eriksen 1996; Weller and Plueddemann 1996).

Schudlich et al (1998) used the Price et al (1987) method to study the seasonal variation in the Ekman layer. They found a coherence at low frequencies (more than 1 day) between the near surface current and the wind (LOTUS experiment).

SADCP (Shipboard Acoustic Doppler Current Profiler, looking downward) have been used in several studies to estimate or separate current components, but mostly in support to LADCP (Lower Acoustic Doppler Current Profiler, looking upward). Comas-Rodriguez et al (2011) used LADCP to compute geostrophic field from a reference level (1000m or 3000m) and SADCP are used to adjust the shallower LADCP and validate the computed transport together with the satellite-derived geostrophy. (Barotropic tidal component is first removed from the ADCP.) Moreover, relative geostrophic velocity is computed using thermal wind and station pairs from LADCP section.

Moreover, SADCP data have been used to choose the reference velocity for the initial geostrophic field of an inverse model in different studies and regions (Joyce et al., 2001; McDonagh et al., 2008).

Consequently, the proposed technique to explore wind driven component in the SISMER SADCP data base would be to:

1- Select data sampling the upper most ocean layers (measurements at least in the first 20m)
2- Select SADCP sampling the local MLD
3- Estimate a reference level and/or reference velocity to be removed to isolate the "wind-driven like" velocity
4- Estimate the coherence between the extracted wind driven velocity and the wind.

The useful data available in the SADCP files are:

-   Time, positions and depth of the measurements;
-   Zonal and meridional absolute velocity
-   Zonal and meridional absolute velocity corrected from tide
-   Zonal and meridional tide velocity (fromTPXO8.0)
-   Zonal and meridional ship velocity

To extract the wind driven component from the SADCP, we have to filter the high frequency of the signal (corrected from tide) and remove a reference velocity ($\vec{U}_{ref}$) to get the $\vec{U}_{ek}$ term of eq. 1.

$$(\vec{U}_{adcp} - \vec{U}_{tide}) = \vec{U}_{ref} + \vec{U}_{ek} + \vec{U}_{inertial} + \vec{U}_{ageo/hf}$$

eq. 1

Hence, we will use the tide corrected absolute velocity and sub sample the time series. We keep the objectives to compare these data with an Ekman model or an OGCM model. So, a time resolution of 1 hour is largely enough as it allows to potentially resolve the tide signal and most of the available wind model variability (for example, ERA interim is a 3h products).

Moreover, we need to remove the high frequency signal (i.e. the two last terms of eq. 1). As the ship is moving, the measured ocean dynamic is different along the ship trajectory. So, averaging the whole time series has no meaning.

We unsuccessfully try to find some station in the data by selecting trajectory segments with ship velocity below 0.05 m.s^{-1} during at least 20 minutes. So, we choose to process the data using rolling average with 6h00, 1 day and 2 days window. We finally don't use the 2 days rolling mean, as the time series are often not long enough. Moreover, some ship routes, as in Figure 9, sample very different dynamics during a small period (here a week). So, a long averaging window is not suitable.
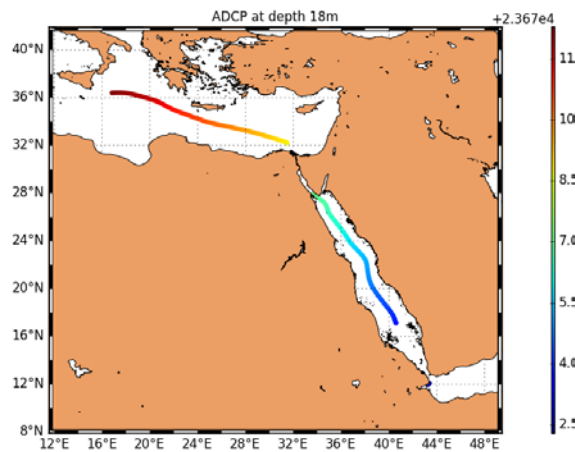

Figure 9: Positions of the TV_DJIBOUTI_TUNIS SADCP measurements

Finally, 5 methods are retained to extract the wind driven signal from the filtered SADCP:

- Subtract the geostrophy derived from altimetry: $\vec{U}_{ref} = \vec{U}_{geo}$
  This is a surface signal removed to all the SADCP levels. Data are taken from CMEMS SEALEVEL_GLO_PHY_L4_REP_OBSERVATIONS_008_047 products (CMEMS-SL-QUID-008-032-051). This is a daily product at ¼° spatial resolution.
- Subtract a 3D geostrophic signal from the Global ARMOR3D L4 Reprocessed data: $\vec{U}_{ref} = \vec{U}_{geo3D}$
  This is a baroclinic signal combining geostrophy from altimetry and in situ T,S profils (CMEMS-GLO-QUID-001-021). These are weekly products with a ¼° resolution.
- Remove the vertical mean velocity at each location.
- Remove a deep velocity reference below the MLD. MLD is estimated from the REP ARMOR3D products. The depth of the reference velocity is taken as the maximum between the MLD and a chosen depth. We chose 50m and 100m as reference depth.

Example of the TR_ABIPDA SADCP is shown in Figure 10 to Figure 13. Figure 10 shows the impact of the filter on the velocity measurements corrected from tide. As the filter is applied on a trajectory, both spatial and temporal high frequencies are filtered. Considering the spatial filtering, it highly depends on the ship velocity: faster the ship is sailing, larger are the filtered spatial patterns.

Figure 11 to Figure 13 show the resulting residual velocity obtained from the 5-different processing and expected to be a wind driven signal. First, the residual velocity obtained by removing the geostrophic signals (surface or 3D) are very similar (Figure 11). The magnitude of zonal residual velocity in the first 100m is similar to the total signal, especially in the first part of the trajectory. In the meridional direction, the difference with the total signal is clearer, even if for some position the two signals are near equal (beginning of the trajectory). This is not expected from an Ekman signal. The position of the ship during the beginning of the campaign is very coastal. Geostrophy is not well resolved and this possibly introduces some error in the residual velocity. But, considering open sea trajectories still show unrealistic residual velocity compared to expected wind driven motion.

Figure 12 shows the residual velocity from the mean velocity reference (hereafter MV). Amplitude of the signal is clearly lower than the total signal. This residual velocity is close to the one obtained by removing the 100m depth reference velocity (Figure 13, lower plots). In this last figure, we see the sensitivity of the depth of the reference level. The residual velocity reaches a zero value at the chosen depth reference (50m or 100m). Assuming that this residual velocity is a wind driven motion, this is a spurious result, as the zero-velocity depth may correspond to the bottom of the Ekman layer.

The considerations above can be applied to all the selected SADCP of Appendix B -.
Hence, using a mean velocity as reference seems to be the best option.
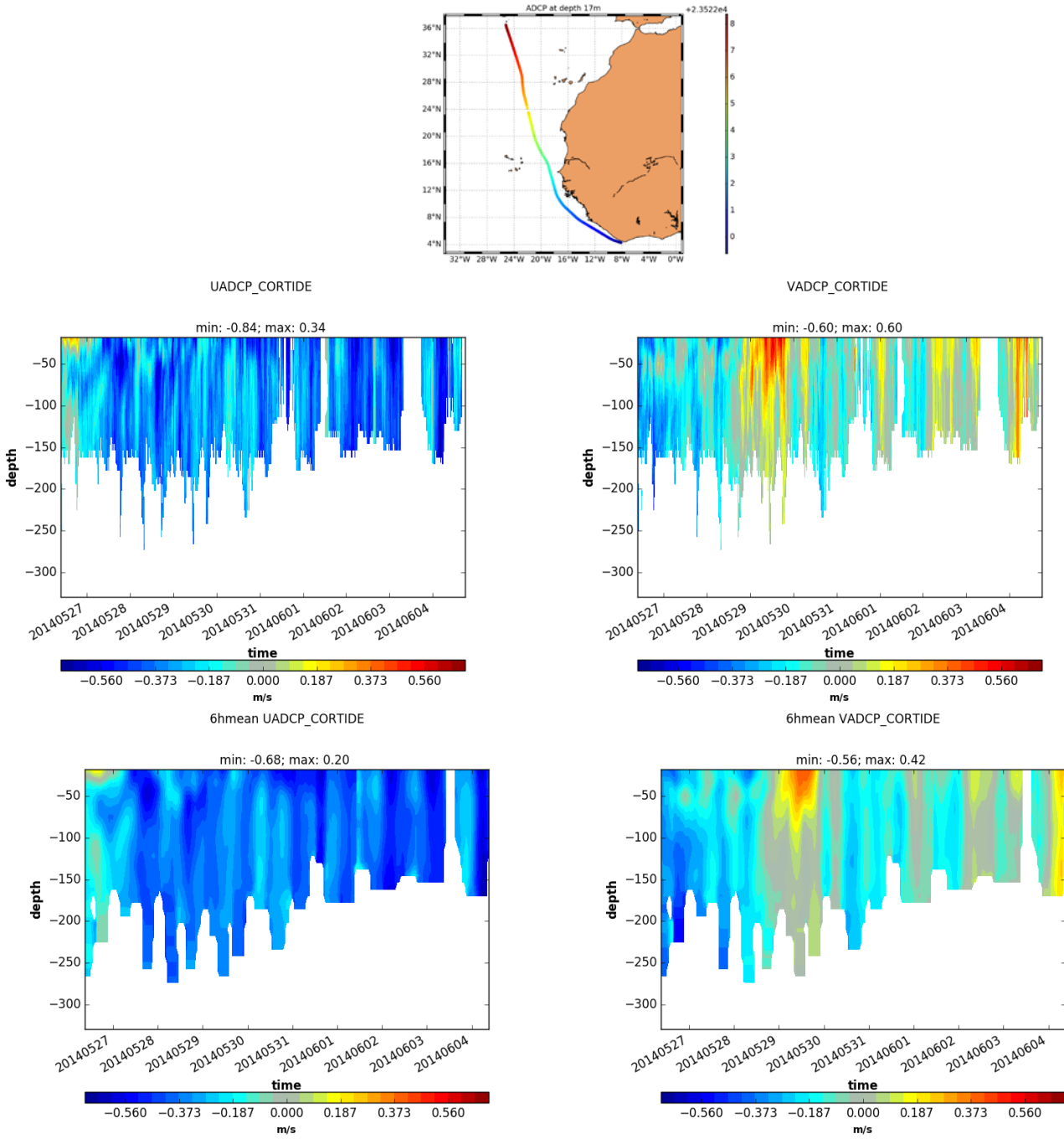
Figure 10: zonal (left) and meridional (right) tide corrected velocity of SADCP TR_ABIPDA_150WT_1E. Upper plots are raw data from the database, lower plots are filtered data (6h window).
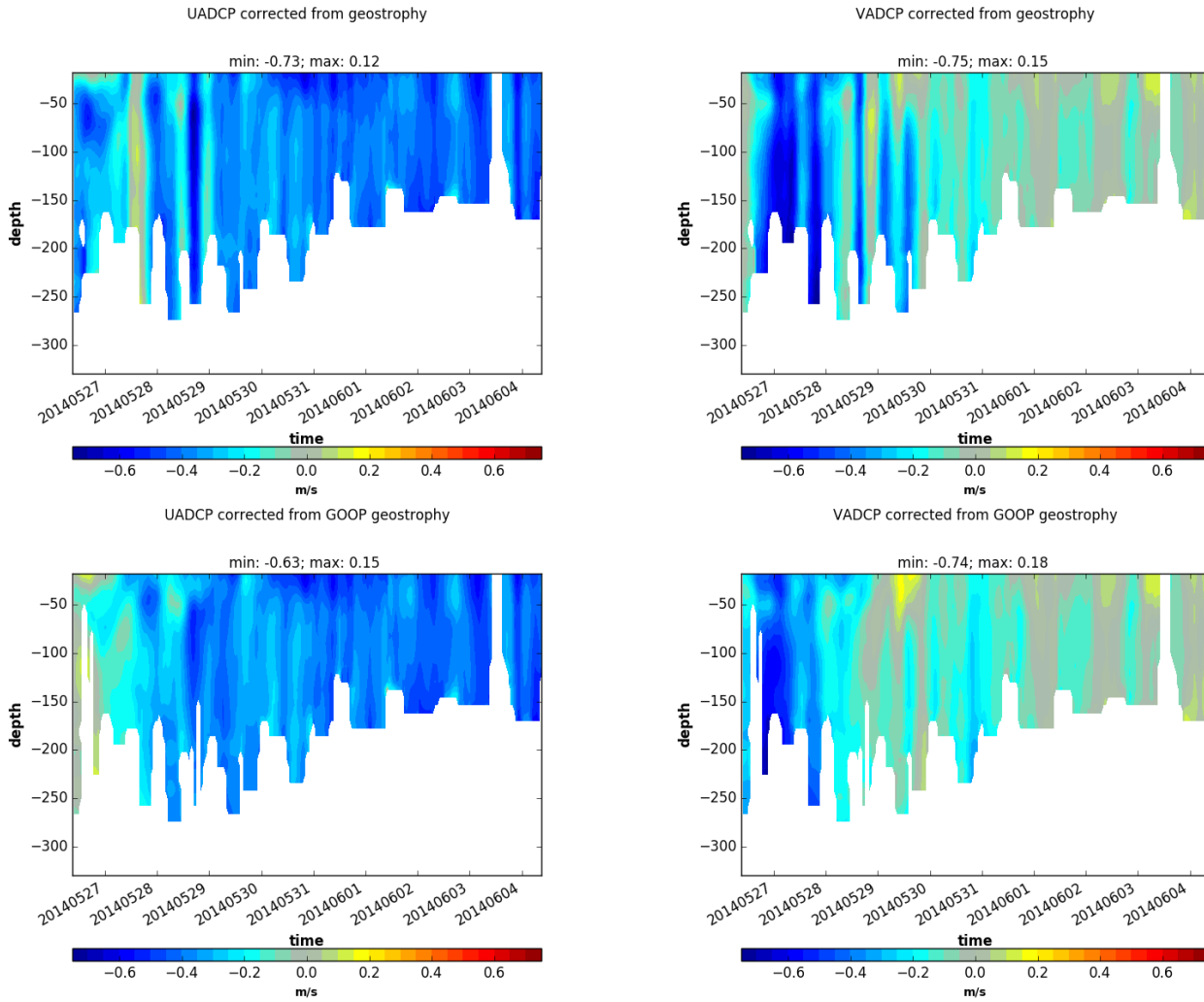
Figure 11: zonal (left) and meridional(right) corrected velocity of SADCP TR_ABIPDA_150WT_1E (6h filter applied). Upper plot: the geostrophy from altimetry has been removed from the tide corrected SADCP velocity. Lower plot, the 3D geostrophic velocity is removed.
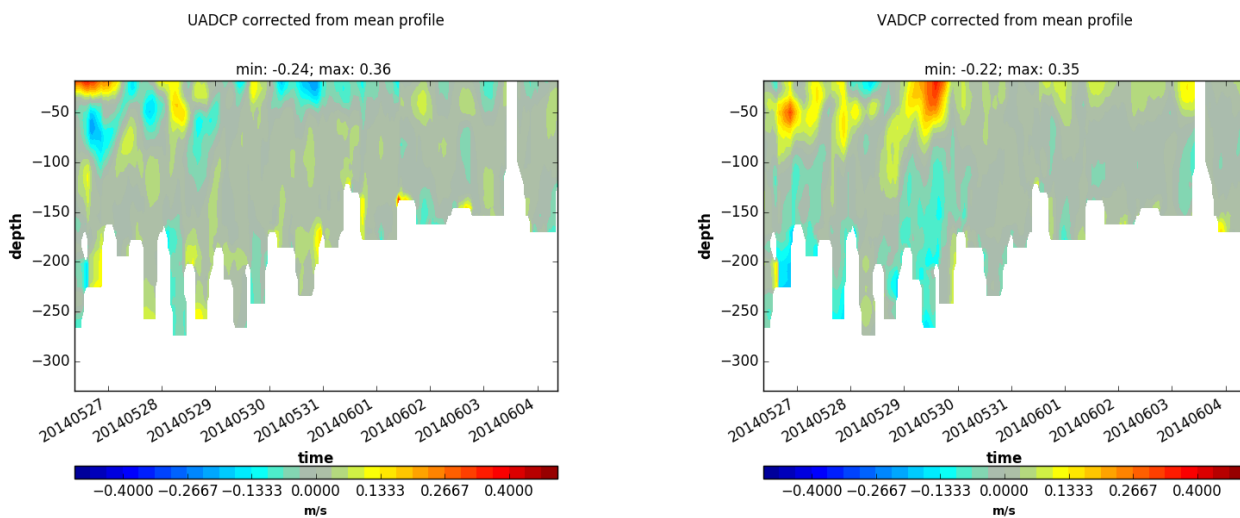
Figure 12: zonal (left) and meridional(right) corrected velocity of SADCP TR_ABIPDA_150WT_1E (6h filter applied). The vertical mean velocity is removed from the tide corrected SADCP velocity
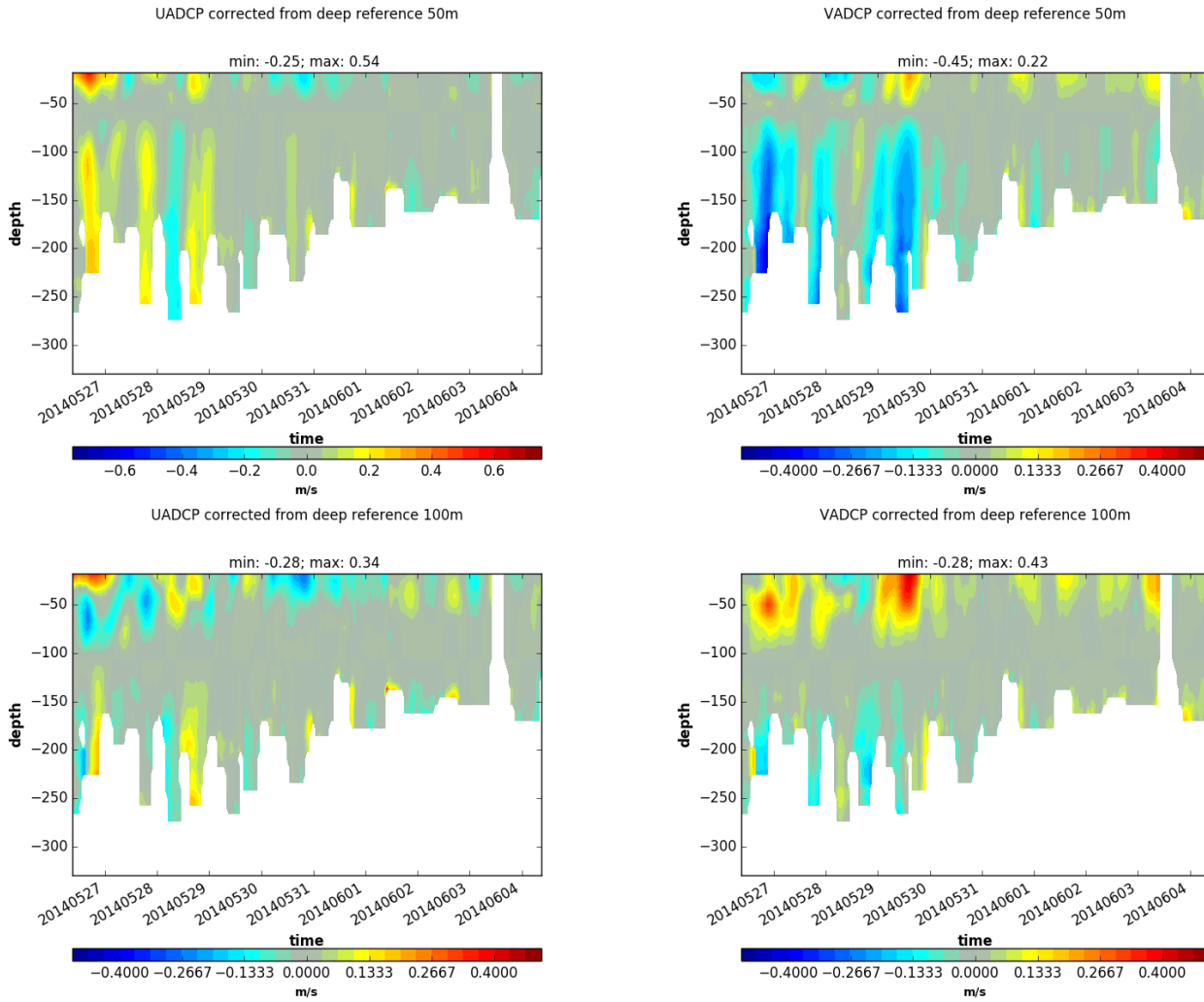
Figure 13: zonal (left) and meridional(right) corrected velocity of SADCP TR_ABIPDA_150WT_1E (6h filter applied). Upper plot: the 50m velocity has been removed from the tide corrected SADCP velocity. Lower plot, the 100m velocity is removed.

3.2.1. Ekman spiral observation

We now explore the vertical profile of the residual velocity to find some spiral like structures. Figure 14 shows the theoretical behaviour of the wind driven motion as described by Ekman; 1905. The surface residual velocity is directed to the right (left) of the wind in the northern (southern) hemisphere respectively. The residual velocity decreases with depth and continues to rotate in the same direction.
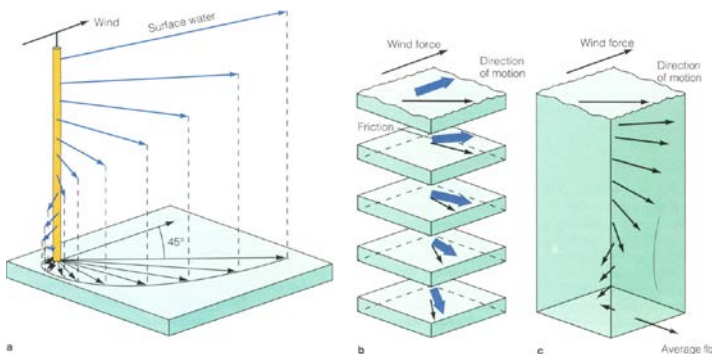
Figure 14: Current profile in the upper layer induced by the Ekman spiral (northern hemisphere).

19

A lot of profiles have been checked and not only for the MV corrected residual velocity. We are able to find some spiral like profiles in almost 1/3 of the 61 selected SADCP. Examples are shown in Figure 15. A common result is that the spiral motion mainly stops between 50 and 70m.
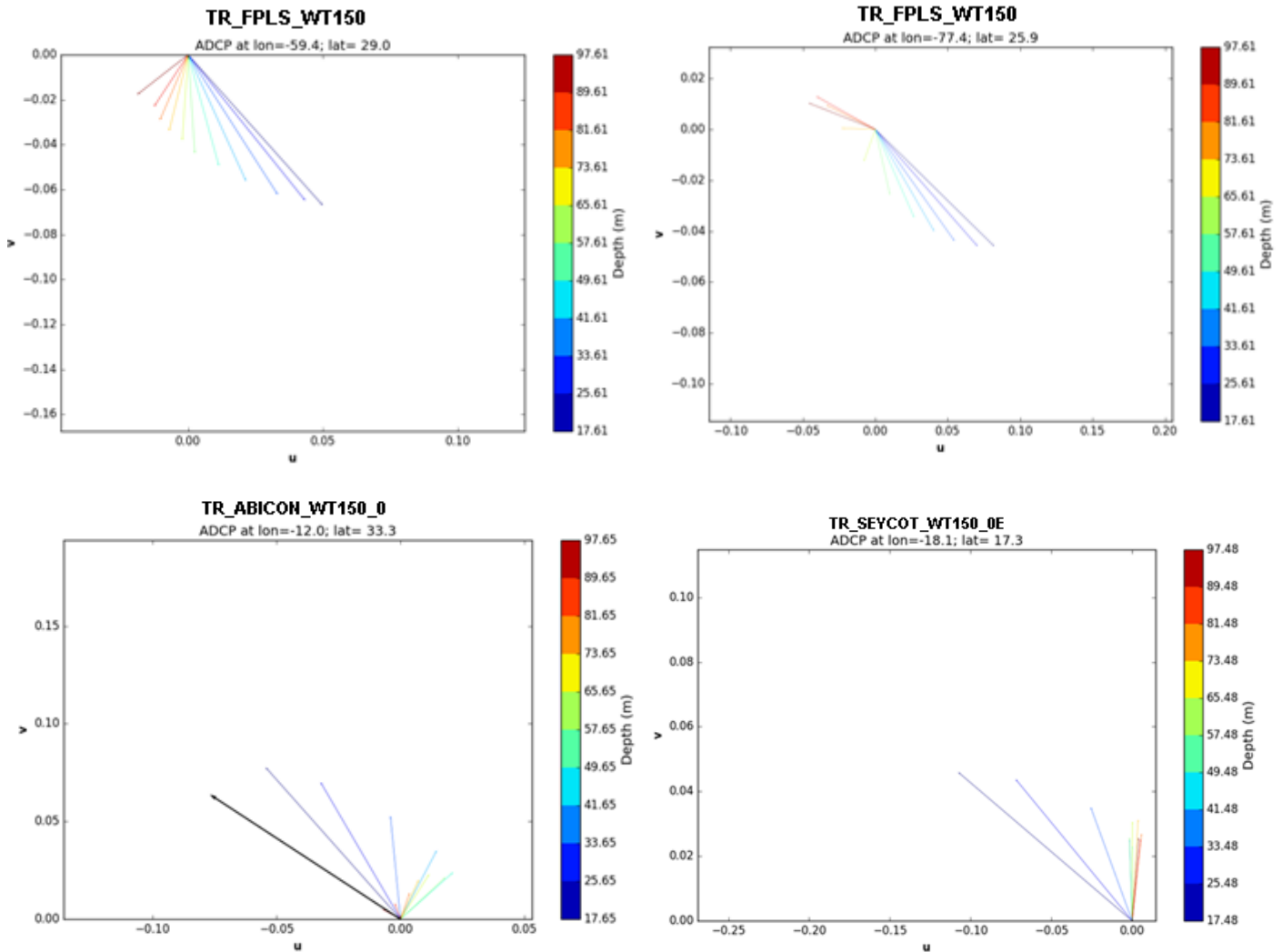
Figure 15: Examples of spiral like profiles at 4 positions of 3 different SADCP. Color scale is for the depth of the velocity. Black arrow indicates the direction of the wind.

However, we are not able to identify spiral profiles at each position of the SADCP measurement, and at some positions the rotation is not in the expected direction. So, the question arises to know if this signal is only wind driven.

3.2.2. Comparison with Ekman model

To estimate the coherence with a wind driven motion, we compare the SADCP MV residual velocity to a 3D Ekman model. This model has been run at CLS and is similar to the OSCAR system described in Bonjean and Lagerloef (2002). This is a ¼° horizontal resolution model, with 5m vertical resolution from the surface down to 135m. It is forced by ECMWF ERA-interim 6h wind stress and it uses a constant viscosity coefficient on the vertical. This viscosity depends on the wind (see Bonjean and Lagerloef (2002) for more details.) A 2 years simulation has been made from 2014 to end of 2015. The Ekman currents have been collocated to 2014 and 2015 SADCP tracks.

Direct comparison between Ekman model and SADCP MV residual velocity have been made, as their vectorial correlation with wind.

15 SADCP are studied. The Ekman model does not compare to the MV residual velocity. Direction and intensity of the 2 products are different. SADCP velocity is greater than the Ekman current (up to one order of magnitude) and we often find opposite direction in the 2 fields.

Percent of the RMS difference (relative to the RMS of the SADCP MV residual velocity) is close (or greater) to 100%.

The vectorial correlations mainly show a vertical rotation in both case, but sense or rotation speed are not comparable (theory as described on Figure 14: Current profile in the upper layer induced by the Ekman spiral (northern hemisphere). is not always verified in the SADCP MV residual velocity) Hence, we probably cannot properly extract the wind driven component from the SADCP with the above processing.

3.3. Using SADCP for ocean current products validation

We now use the SADCP velocity corrected from tide to compare with geostrophic velocity from ARMOR3D and total velocity from Mercator Ocean global model. As the ARMOR3D are weekly data and Mercator Ocean 3D data is daily, we interpolate these fields onto the filtered SADCP positions (6 hours, 1 day and 2 days windows.)
Comparisons are then perform including:
- Statistics along the trajectory (mean difference profile, RMS of differences, percent of RMS differences relative to SADCP RMS);
- Taylor plot for each level;
- Current roses;
- Map of superimposed SADCP and products current arrows.

3.3.1. ARMOR3D geostrophic velocity

As said previously, 3D geostrophic velocity from the ARMOR3D system are weekly products, on a ¼° grid. So, we don't expect a good concordance in variability. However, the ARMOR3D velocities compare well with the SADCP. 64% of the computed % of RMS difference show value below 100% for one or two of the velocity components, while the remaining 35% show larger values or the SADCP data are too sparse.

Example of TR_FPLS_WT150_0 SADCP is shown in Figure 16. This is a 20 days cross North Atlantic route. Even if the SADCP signal is a total signal corrected from tide (eq. 1), the 3D geostrophic signal matches quite well the in-situ measurements with an overall % of RMS differences around 40% on the water column.

The SADCP data are in this case useful to identify the regions where geostrophy is dominant in the total signal and validate the 3D geostrophic current.

There is no clear evidence on which filter is the more relevant to compare with the 3D geostrophy, but in general the 6 hours or 1 day rolling mean window gives the best comparison to the SADCP. The 1 day mean rolling window data are of course smoother and we could have expected they better fit the weekly variability of the 3D geostrophy. But, the vessels move fast (generally between 3 to 5 m/s), and therefore the spatial variability dominates the signal much more than the temporal variability. An along trajectory

spatial rolling mean window has been testing on the data, but no significant improvement is found on the validation results.
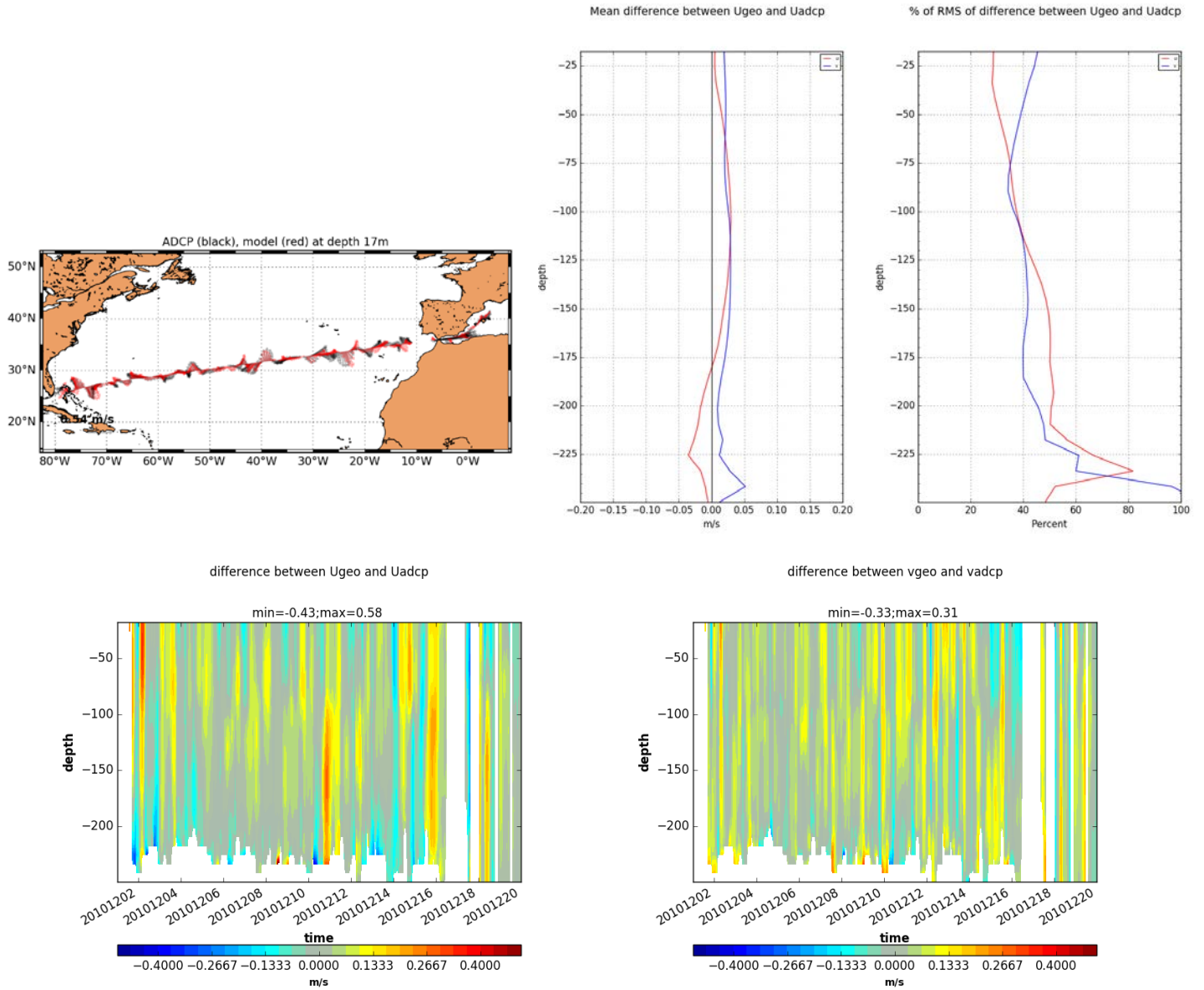
Figure 16: Comparison between TR_FPLS_WT150_0 SADCP currents (corrected from tide) and collocated ARMOR3D geostrophy processed with a 6 hour rolling mean window. Current arrows at 52m (upper left) of the 2 fields show the ship trajectory. Mean difference for u and v and mean % of RMS differences are shown in upper middle and upper right plots. The u (left) and v (right) differences along the SADCP track are shown in the lower plots.

3.3.2. CMEMS global model

We processed the daily 1/12° u and v GLOBAL_ANALYSIS_FORECAST_PHY_001_024 products from CMEMS to be compared with the filtered SADCP data. Hence, the 3D velocity fields are interpolated at the position, depth and time of the filtered SADCP measurements.

As said in the previous report, we have shown some inconsistency between the model and one ADCP (TR_ABIPDA), probably due to a default in the ship velocity correction. Hence, this basic comparison is a tool to validate the first step of the SADCP processing, according to the local dynamics understanding.

We also investigate the possibility to extract a wind driven component from the model velocity field, but we faced the same issue as for the SADCP processing. Using a mean velocity or a 100m depth reference velocity seems to provide the best results considering the number of observed spiral like vertical profiles. But we have no guaranty that this is a fully wind driven dynamics.

Direct comparison between the processed model and SADCP fields shows some good statistical results (correlation, mean difference and standard deviation, see Figure 17). Particular attention has to be given to the signal variability, as in many cases, the % of the RMS of the differences is greater than 100%. When increasing the rolling mean window, this error is mainly not corrected. Again, a spatial filtering is probably suitable according to the model spatial resolution.
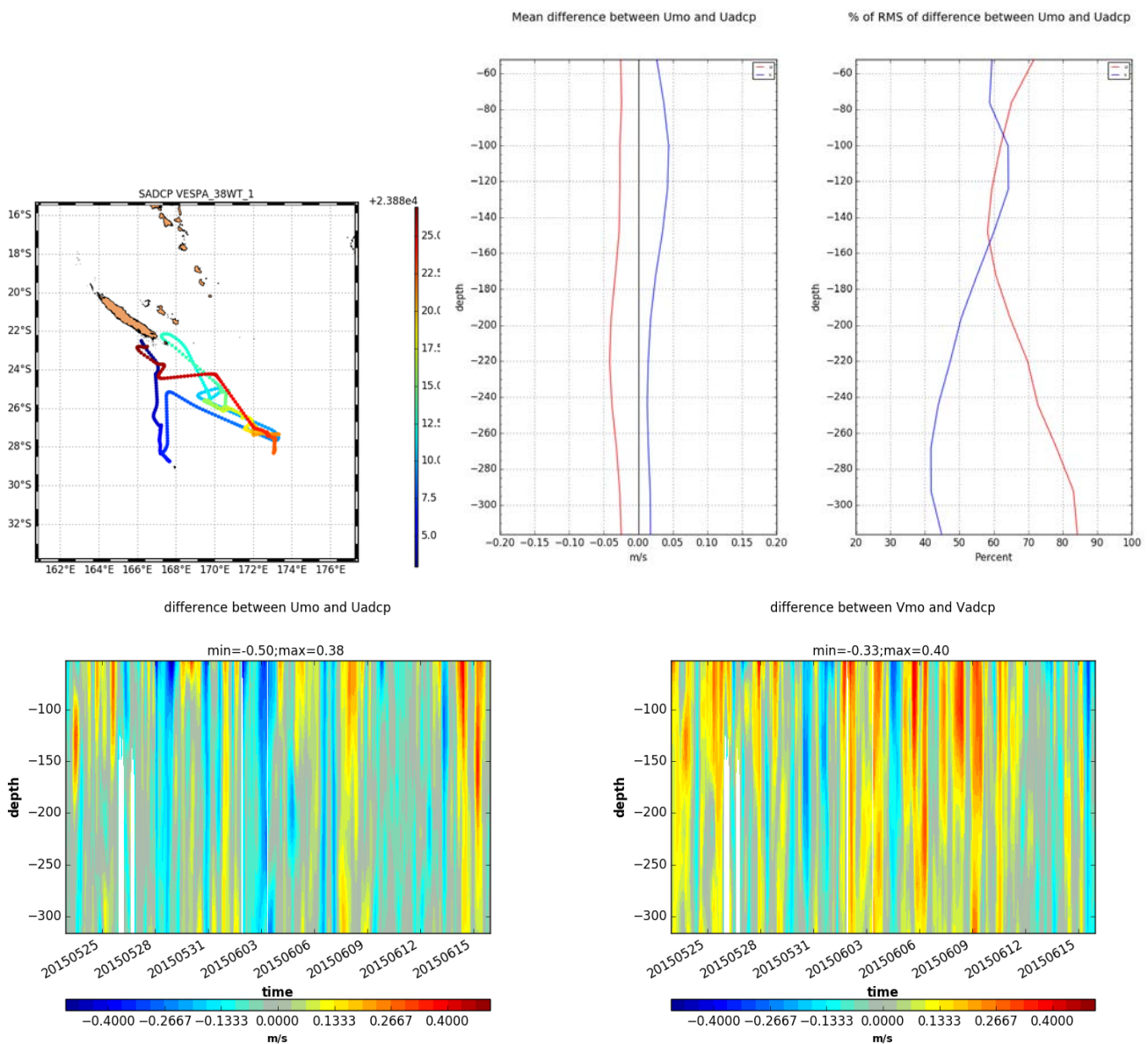

Figure 17: Comparison between VESPA_38WT_1 SADCP currents (corrected from tide) and collocated CMEMS global model processed with a 6-hours rolling mean window. Mean difference for u and v and mean % of RMS difference are shown in upper middle and upper right plots. The u (left) and v (right) differences along the SADCP track are shown in the lower plots.

3.4. Recommendations for SADCP use

We faced many issues using the Sismer SADCP data base. As far as we are concerned and in the range of applications described in this document, too many confusing information are provided in the Netcdf files.

For validation purposes or case studies, the main useful variables are:
- **LONGITUDE, LATITUDE, DEPH, JULD**: position, depth and date of the measurements
- **UVEL_SHIP, VVEL_SHIP**: eastward and northward ship velocity
- **EVEL_ADCP**: absolute ADCP current velocity error
- **UVEL_ADCP, VVEL_ADCP, WVEL_ADCP**: eastward, northward and vertical ADCP absolute current velocity
- **BATHY:** Gebco digital atlas bathymetry
- **U_TIDE, V_TIDE**: eastward and northward tide velocity (from model TPXO8.0).
- **UVEL_ADCP_CORTIDE, VVEL_ADCP_CORTIDE:** eastward and northward ADCP current velocity corrected from tide.

Most of the other variables are related to the instrument and only useful to experts.
In one hand, a simplification of the file contain could be beneficial together with a full description and documentation.
On the other hand, additional information could be added:
- FES 2014 tide velocity for comparison
- In situ or collocated atmospheric data from model (10m wind, wind stress)

When relevant, some station files could be extracted from the SADCP files and clearly identified.

4. Conclusion

In a first chapter, we have highlight the usefulness of the drifting buoy velocity dataset in the Atlantic Ocean to validate a new velocity dataset produced from the synergy of altimeter data and Sea Surface Temperature information. As a perspective, the drifter velocities could now be used to further improve the optimally merged SSH/SST dataset through a multivariate objective analysis.

In a second chapter, we have investigated a Ship ADCP database and its relevance to describe wind driven signal and validate currents from model. This last part is not fully concluding as the full SADCP signal is complex and complicated to analyse. But this study highlights some perspectives on the pre-processing of these data for model validation purposes and provides some recommendations to the data providers to ease the understanding and the use of these products.

We have shown the usefulness of the drifters and SADCP data in captor synergy technics and in procedure for model velocity validation.

5. References

Bonjean F. and G.S.E. Lagerloef , 2002: Diagnostic Model and Analysis of the Surface Currents in the Tropical Pacific Ocean. J. Phys. Oceanogr., 32, 2938-2954

Chereskin, T. K., 1995 : Direct evidence of an Ekman balance in the California Current. Journal of Geophysical Research, Vol. 100, C9, 261-269.

CMEMS-GLO-QUID-001-021: Quality Information Document, http://marine.copernicus.eu/documents/QUID/CMEMS-GLO-QUID-001-021.pdf

CMEMS-SL-QUID-008-032-051 : Quality Information Document, http://marine.copernicus.eu/documents/QUID/CMEMS-SL-QUID-008-032-051.pdf

Comas-Rodríguez, I., A. Hernández-Guerra, E. Fraile-Nuez, A. Martínez-Marrero, V. M. Benítez-Barrios, M. D.Pérez-Hernández, and P. Vélez-Belchí , 2011: The Azores Current System from a meridional section at 24.5°W, J. Geophys.Res., 116, C09021, doi:10.1029/2011JC007129.

Comas-Rodríguez, I., A. Hernández-Guerra, and E. McDonagh, 2010: Referencing geostrophic velocities using ADCP data at 24.5°N (NorthAtlantic), Sci. Mar., 74(2), 331–338, doi:10.3989/scimar.2010.74n2331.

Davis, R. E., R. deSzoeke, and P. P. Niiler, 1981: Variability in the upper ocean during MILE, II, Modeling the mixed layer response. Deep Sea Res., Part A, 28A, 1453-1475.

Ekman, V. W., 1905: On the influence of the earth's rotation on ocean-currents, Ark. Mat. Astron. Fys., 2, 1-52, 1905.

IFREMER / IDM/SISMER, SHOM, 2014 : ADCP de coque des navires océanographiques français. IFREMER / IDM/SISMER. http://doi.org/10.12770/60ad1de2-c3e1-4d33-9468-c7f28d200305

Joyce, T. M., A. Hernández-Guerra and W. M. Smethie Jr., 2001: Zonal circulation in the NW Atlantic and Caribbean from a meridional World Ocean Circulation Experiment hydrographic section at 66°W. J. Geophys. Res., 106(C10): 22,095-22,113.

Lee, C. M., and C. C. Eriksen, 1996: The subinertial momentum balance of the North Atlantic subtropical convergence zone. J. Phys. Oceanogr., 26, 1690–1704.

McDonagh, E., H. Bryden, B. King, and R. Sanders, 2008: The circulation of the Indian Ocean at 32°S, Prog. Oceanogr., 79(1), 20–36, doi:10. 1016/j.pocean.2008.07.001.

Pollard, 1991: Forced ocean response during the Frontal Air–Sea Interaction Experiment. J. Geophys. Res., 96, 8611–8638.

Price, J. F., R. A. Weller, and R. R. Schudlich, 1987: Wind-driven ocean currents and Ekman transport, Science, 238, 1534-1538.

Price, J. F., R. A. Weller, and R. R. Schudlich, 1987: Wind-driven ocean currents and Ekman transport. Science, 238, 1534–1538.

Rio, M.-H., S. Mulet, and N. Picot, 2014: Beyond GOCE for the ocean circulation estimate: Synergetic use of altimetry, gravimetry, and in situ data provides new insight into geostrophic and Ekman currents, Geophys. Res. Lett., 41, doi:10.1002/2014GL061773.

Rio, M-H, R. Santoleri, R. Bourdalle-Badie, A. Griffa, L. Piterbarg, G. Taburet, 2016: Improving the altimeter derived surface currents using high-resolution Sea Surface Temperature data: A feasibility study based on model outputs. Journal of Atmospheric and Oceanic Technology, Vol. 33, DOI: 10.1175/JTECH-D-16-0017.1.

Rio, M-H, R. Santoleri (in premaration) : Improved global surface currents from the merging of altimetry and Sea Surface Temperature data. Paper to be submitted in the "Ocean currents from Space" special issue from Remote Sensing of Environment.

Schudlich, R. R., J. F. Price , 1998: Observations of seasonal variation in the Ekman layer. J. Phys. Oceanogr., 28, 1187-1204.

Tanne, A., 2016: Profil vertical de viscosité dans un modèle d'Ekman 3D, rapport de stage M2.

Weller, R. A., , D. L. Rudnick, C. C. Eriksen, K. L. Polzin, N. S. Oakey, J. W. Toole, R. W. Schmitt, and R. T.

Weller, R. A, and A. J. Plueddemann, 1996: Observations of the vertical structure of the oceanic boundary layer. J. Geophys. Res., 101, 8789–8806.

Wijffels, S., E. Firing, and H. L. Bryden, 1994: Direct observations of the Ekman balance at 108N in the Pacific. J. Phys. Oceanogr., 24, 1666–1679.

Appendix A - **Full list of SADCP for 2001-2017**

Year of acquisition	Public cruises	By ships	Non publicly available cruises
2001	8	6 ATALANTE 2 SUROIT	7
2002	12	3 ATALANTE 4 SUROIT 5 THALASSA	2
2003	6	2 ATALANTE 4 SUROIT	2
2004	20	1 ATALANTE 5 SUROIT 4 THALASSA 10 BB	0
2005	37	13 ATALANTE 12 SUROIT 1 THALASSA 11 BB	1
2006	57	14 ATALANTE 12 SUROIT 1 THALASSA 20 BB 1 MS MERRIAN 9 PP	1
2007	57	13 ATALANTE 10 SUROIT 1 THALASSA 15 BB 3 ANTEA 15 PP	0
2008	33	7 ATALANTE 1 SUROIT 4 ANTEA 17 BB 4 PP	3
2009	32	1 ATALANTE 7 SUROIT 18 BB 6 PP	4
2010	61	6 ATALANTE 7 SUROIT 38 BB 1 ANTEA 9 PP	2
2011	27	3 ATALANTE 9 SUROIT 2 THALASSA 7 BB	

		6 PP	
2012	35	5 ATALANTE 6 SUROIT 2 THALASSA 10 BB 12 PP	
2013	46	6 ATALANTE 7 SUROIT 8 PP 25 BB	2
2014	46	5 ATALANTE 6 SUROIT 4 THALASSA 23 BB 8 PP	3
2015	20	8 ATALANTE 5 THALASSA 7 PP	20 (from the French Navy)
2016	20	11 ATALANTE 4 THALASSA 5 PP	2 (from the French Navy)
2017	13	3 ATALANTE 3 THALASSA 7 PP	1 (from the French Navy)

Appendix B - List of selected SADCP for 2010-2015

ADCP_name	date_deb	date_fin	nb_depth	depth_deb	depth_fin	resolution
ASPEX2_BB150_0E	13/05/2010	19/05/2010	40	17.460	329.5	8
TR_PDGLS_WT150_0E	10/08/2010	16/08/2010	40	17.570	329.6	8
TR_LSFP_WT150_0_osite	09/10/2010	27/10/2010	40	17.550	329.5	8
TR_FPLS_WT150_0_osite	01/12/2010	20/12/2010	40	17.610	329.6	8
TR_LHATL_150K_0_osite	17/10/2010	24/10/2010	45	18.770	370.8	8
TR_SEYCOT_WT150_0E	24/03/2011	09/04/2011	40	17.480	329.5	8
fr21_leg1	03/05/2011	20/05/2011	40	17.670	329.7	8
fr21_leg2	23/05/2011	28/05/2011	40	17.670	329.7	8
TR_DAKPDA_WT150_0_osite	16/06/2011	21/06/2011	40	17.610	329.6	8
TR_LHASEY_WT150_0_osite	30/07/2011	06/08/2011	40	17.570	329.6	8
TR_HERSEY_WT150_0E	26/10/2011	28/10/2011	40	17.570	329.6	8
ERATO_150K_WT_0_osite	07/05/2011	17/05/2011	45	18.780	370.8	8
TR_BREPGT_150KWT_0_osite	19/10/2011	03/11/2011	45	18.760	370.8	8
PROTEUSDUNES11_150KWT_0_osite	01/09/2011	06/09/2011	65	14.990	271.0	4
PROTEUS11_L1_150_0_osite	19/09/2011	26/09/2011	64	14.240	266.2	3
TV_MALTE_DJIBOUTI_150WT_0_osite	20/02/2011	24/02/2011	40	18.700	330.7	8
PHYSINDIEN11L1_150WT_0_osite	26/02/2011	02/03/2011	40	18.740	330.7	8
PHYSINDIEN11L3_150WT_0_osite	28/03/2011	31/03/2011	40	18.740	330.7	8
TVTREUIL_WT150_0_osite	14/07/2012	20/07/2012	40	17.530	329.5	8
TR_ABISEY_150_0_osite	03/02/2012	13/02/2012	45	18.730	370.7	8
OWEN_150KWT_1	14/03/2012	27/03/2012	40	18.740	330.7	8
MOCOSED_2012_150_0_osite	02/03/2012	18/03/2012	45	18.790	370.8	8
ULYSSE_150K_WT_1	05/11/2012	24/11/2012	45	18.760	370.8	8
TR_LISATH_150_0_osite	27/10/2012	02/11/2012	45	18.730	370.7	8
TVGMOS2_150_0_osite	24/09/2012	05/10/2012	45	18.750	370.8	8
PROTEUS_DUNES_LEG2_150_1	11/10/2012	19/10/2012	65	15.010	271.0	4
TVGMOS_150_0_osite	06/04/2012	12/04/2012	45	18.740	370.7	8
TR_SEYBRE_150_0_osite	05/12/2012	11/12/2012	45	18.730	370.7	8
PROTEUS_DUNES_LEG3_150_0_osite	21/10/2012	23/10/2012	45	18.760	370.8	8
PROTEUS_DUNES_LEG1_150_1	08/10/2012	11/10/2012	65	15.000	271.0	4
TV_HERAKLION_DJIBOUTI_150WT_1E	11/02/2012	18/02/2012	40	18.690	330.7	8
TV_SALALAH_ABUDHABI_150BT_1E	28/03/2012	31/03/2012	64	14.670	266.7	4
fr22_leg1	21/03/2012	01/04/2012	40	17.550	329.5	8
fr22_leg2	05/04/2012	18/04/2012	40	17.650	329.6	8
fr22_leg3	21/04/2012	30/04/2012	40	17.610	329.6	8
TR_ABICON_WT150_0_osite	22/06/2013	04/07/2013	40	17.650	329.6	8
TR_CATSEY_150_0_osite	26/10/2013	28/10/2013	40	17.570	329.6	8
TR_SEYCAT_150_WT_0_osite	28/09/2013	30/09/2013	40	17.570	329.6	8
TR_LHACOR_150_0_osite	07/09/2013	10/09/2013	55	18.730	450.7	8
TV_INFO_150_0_osite	06/11/2013	14/11/2013	55	18.730	450.7	8
COMET_150K_WT_1	26/02/2013	01/03/2013	70	14.640	290.6	4
TV_MINDELO_DAKAR_150WT_1	30/03/2013	31/03/2013	40	18.710	330.7	8
RAZ_BLANCHARD_15_150BT_1	05/07/2013	06/07/2013	64	14.640	266.6	4
LADEROUTE2_150BT_1	18/07/2013	27/07/2013	64	14.630	266.6	4
LADEROUTE3_150BT_1	13/08/2013	21/08/2013	64	14.650	266.6	4
PROTEUSDUNES2013_150BT_1	27/08/2013	10/09/2013	64	14.650	266.6	4
TR_SEYDAK_150WT_0E	29/03/2014	07/04/2014	40	17.480	329.5	8
TR_ABIPDA_150WT_1E	26/05/2014	04/06/2014	40	17.650	329.6	8
TR_PDASEY_150WT_0E	22/06/2014	28/06/2014	40	17.550	329.5	8
SOCADEN_2014_BB_150K_WT_1E	26/02/2014	03/03/2014	40	18.740	330.7	8
TV_MASCATE_DIEGO_2014_BB_150K_WT_1E	05/06/2014	15/06/2014	40	18.780	330.8	8
TV_DZAOUDZI_MORONI_2014_BB_150K_WT_1	02/08/2014	03/08/2014	40	18.740	330.7	8
TV_MORONI_ANSTI_2014_BB_150K_WT_1	28/08/2014	29/08/2014	40	18.740	330.7	8
TV_ANTSI_LOGONI_2014_BB_150K_WT_1	03/09/2014	05/09/2014	40	18.750	330.8	8
TV_LONGONI_MAHE_2014_BB_150K_WT_1E	04/10/2014	08/10/2014	40	18.750	330.8	8
TV_DJIBOUTI_TUNIS_2014_BB_150KWT_1E	24/10/2014	03/11/2014	40	18.770	330.8	8
TV_TUNIS_BREST_2014_BB_150K_BT_1	09/11/2014	12/11/2014	40	18.720	330.7	8
fr25	18/03/2015	15/04/2015	70	16.270	292.3	4
TR_BREGDA_150BT_1	03/02/2015	07/02/2015	65	15.170	271.2	4
TR_GDABRE_150BT_1E	16/03/2015	20/03/2015	65	15.160	271.2	4
TR_SEYLON_2015_PP_150K_WT_1E	19/10/2015	08/11/2015	55	18.760	450.8	8